Published online 23 March 2017

Nucleic Acids Research, 2017, Vol. 45, No. 11 ***e105***
doi: 10.1093/nar/gkx200

Orientation-dependent FRET system reveals differences in structures and flexibilities of nicked and gapped DNA duplexes

Hiromu Kashida[1,2,*], Ayako Kurihara[1], Hayato Kawai[1] and Hiroyuki Asanuma[1,*]

[1]Graduate School of Engineering, Nagoya University, Furo-cho, Chikusa-ku, Nagoya 464-8603, Japan and
[2]PRESTO, Japan Science and Technology Agency, 4-1-8 Honcho, Kawaguchi, Saitama 332-0012, Japan

Received October 28, 2016; Revised March 09, 2017; Editorial Decision March 13, 2017; Accepted March 17, 2017

ABSTRACT

Differences in structures and flexibilities of DNA duplexes play important roles on recognition by DNA-binding proteins. We herein describe a novel method for structural analyses of DNA duplexes by using orientation dependence of Förster resonance energy transfer (FRET). We first analyzed canonical B-form duplex and correct structural parameters were obtained. The experimental FRET efficiencies were in excellent agreement with values theoretically calculated by using determined parameters. We then investigated DNA duplexes with nick and gaps, which are key intermediates in DNA repair systems. Effects of gap size on structures and flexibilities were successfully revealed. Since our method is facile and sensitive, it could be widely used to analyze DNA structures containing damages and non-natural molecules.

INTRODUCTION

Structural anomalies in DNA double-helical structures play important roles in biological processes, allowing, for example, DNA repair enzymes to find damaged sites among a huge number of intact base pairs. Recent studies have indicated that DNA-binding proteins can recognize differences in structures and flexibilities of DNA duplexes (1,2). X-ray crystallography and nuclear magnetic resonance (NMR) are powerful tools for analysis of DNA structures, but these techniques require a large amount of sample and are time consuming. Further, the X-ray crystal structures revealed may not reflect the structures found in biological milieu. Förster resonance energy transfer (FRET) is a versatile tool for nucleic acid structural analyses since its efficiency sensitively depends on relative distance and orientation between a donor and an acceptor (3–13). In most FRET-based studies of DNA, only distance dependence has been analyzed since dye orientations are difficult to control, although several groups have succeeded in observing orientation dependence by using DNA scaffolds (14–18). We previously reported a novel FRET system in which donor and acceptor are incorporated into DNA through D-threoninol linkers (19). Using the D-threoninol scaffold, various dyes were incorporated into DNA in fixed orientations (20). The observed FRET efficiencies showed orientation dependence that agreed with theoretical values calculated based on reported parameters for a B-form duplex although difference still remained due to bending caused by A-tract sequences. Here, we applied this FRET system for analyses of DNA double helical structures. In contrast to the previous study, we determined structural parameters of various DNA structures from experimentally determined FRET efficiencies. We first analyzed the canonical B-form double helix by using orientation-dependent FRET and then evaluated nicked and gapped DNA duplexes, which are key intermediates in DNA repair systems (21,22). Not only the structures but also the flexibility of DNA in solution were revealed using orientation-dependent FRET. To the best of our knowledge, differences between both structures and flexibilities of nicked/gapped duplexes are revealed for the first time.

Sequences of oligonucleotides used in this study are shown in Figure 1. Pyrene and perylene were incorporated into DNA via D-threoninol as a donor and an acceptor, respectively. It was difficult to control dye orientation because dyes were usually introduced into terminal or extrahelical positions of DNA. In contrast, molecules can intercalate between base pairs when they are introduced into the middle positions of DNA through D-threoninol (23). Therefore, their orientations can be strictly controlled through stacking interaction with neighboring base pairs. No abasic sites were incorporated at the counter positions of dyes because we have revealed that additional incorporation of dyes do not distort DNA structures. We varied the number of base pairs between the pyrene donor and the perylene acceptor and measured FRET efficiencies. The FRET plot of the

*To whom correspondence should be addressed. Tel: +81 52 789 2538; Fax: +81 52 789 2528; Email: kashida@nubio.nagoya-u.ac.jp
Correspondence may also be addressed to Hiroyuki Asanuma. Tel: +81 52 789 2488; Fax: +81 52 789 2528; Email: asanuma@nubio.nagoya-u.ac.jp

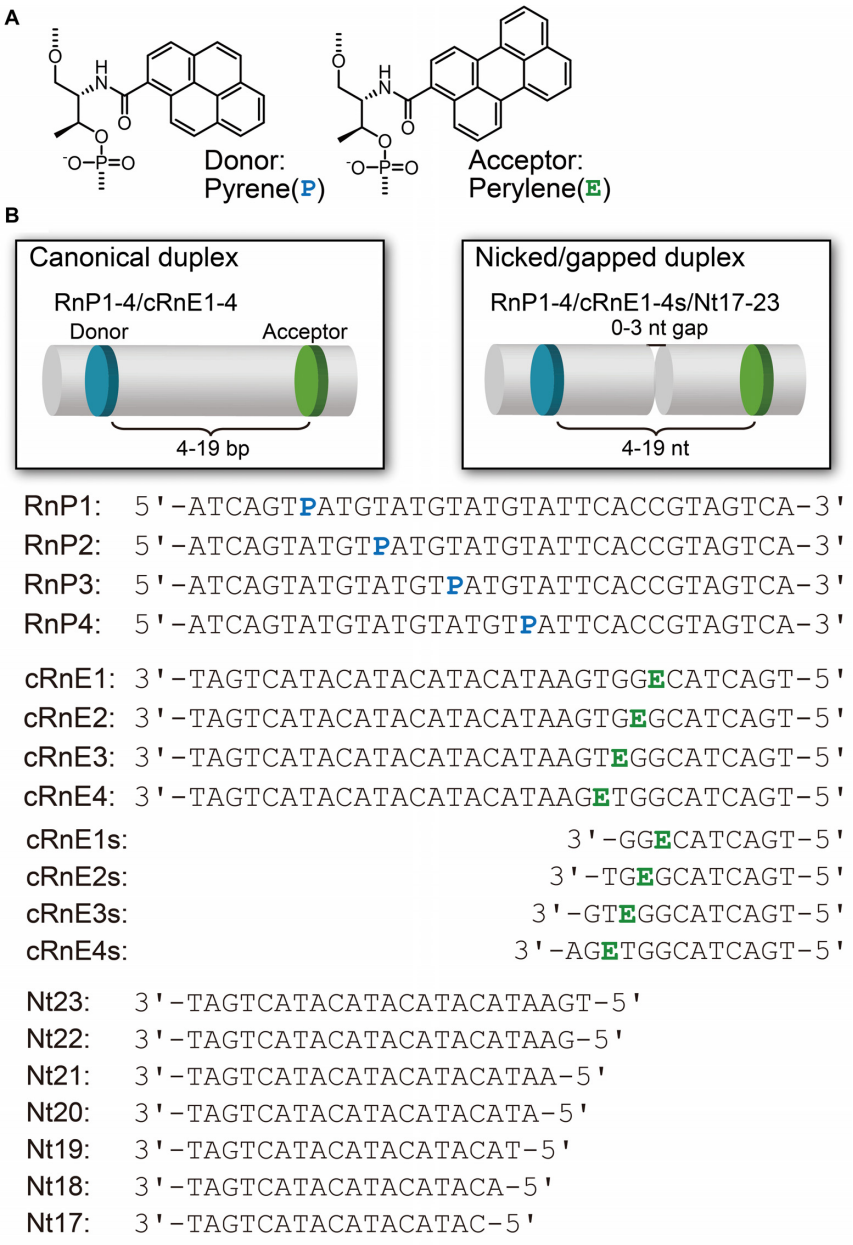

Figure 1. (**A**) Chemical structures of donor and acceptor. (**B**) Sequences of oligonucleotides used in this study. Schematic illustrations of canonical and nicked/gapped duplexes are also shown.

efficiency versus the number of base pairs was then fit to structural parameters obtained based on a cylinder model of the B-form duplex. There are several advantages of our method; (i) detailed structural parameters in solution can be easily obtained by using not only distance dependence but also orientation dependence of FRET. (ii) Since orientation is strictly controlled in our FRET system, experimental FRET efficiencies showed excellent agreement with theoretically calculated values (*vide infra*). Therefore, even bending and flexibility of DNA duplex can be estimated by monitoring deviations from the cylinder model. (iii) Dye pairs with relatively long Förster radius can be used with our method so that large DNA structures can be analyzed.

MATERIALS AND METHODS

Oligonucleotides

All conventional phosphoramidite monomers, Controlled Pore Glass (CPG) columns, reagents for DNA synthesis and Poly-Pak II cartridges were purchased from Glen Research. Other reagents for the synthesis of phosphoramidite monomers were purchased from Tokyo Chemical Industry, Wako and Aldrich. Native oligodeoxyribonucleotides (ODNs) were purchased from Integrated DNA Technologies.

Dye-conjugated ODNs were synthesized on an automated DNA synthesizer (H-8-SE, Gene World) as we reported previously (24,25). ODNs were purified by reversed-

phase HPLC and characterized by MALDI-TOF MS (Autoflex II, Bruker Daltonics) and HPLC.

The MALDI-TOFMS data for the modified DNA were as follows: RnP1: Obsd. 10220 (Calcd. for [RnP1+H$^+$]: 10220). RnP2: Obsd. 10219 (Calcd. for [RnP2 +H$^+$]: 10220). RnP3: Obsd. 10220 (Calcd. for [RnP3 +H$^+$]: 10220). RnP4: Obsd. 10220 (Calcd. for [RnP4 +H$^+$]: 10220). cRnE1: Obsd. 10257 (Calcd. for [cRnE1 +H$^+$]: 10257). cRnE2: Obsd. 10257 (Calcd. for [cRnE2 +H$^+$]: 10257). cRnE3: Obsd. 10257 (Calcd. for [cRnE3 +H$^+$]: 10257). cRnE4: Obsd. 10257 (Calcd. for [cRnE4 +H$^+$]: 10257). AtP1: Obsd. 10297 (Calcd. for [AtP1+H$^+$]: 10300). AtP2: Obsd. 10300 (Calcd. for [AtP2 +H$^+$]: 10300). AtP3: Obsd. 10298 (Calcd. for [AtP3 +H$^+$]: 10300). AtP4: Obsd. 10299 (Calcd. for [AtP4 +H$^+$]: 10300). AtP5: Obsd. 10300 (Calcd. for [AtP5 +H$^+$]: 10300). cAtE1: Obsd. 10168 (Calcd. for [cAtE1 +H$^+$]: 10170). cAtE2: Obsd. 10169 (Calcd. for [cAtE2 +H$^+$]: 10170). cAtE3: Obsd. 10169 (Calcd. for [cAtE3 +H$^+$]: 10170). cRnE1s: Obsd. 3184 (Calcd. for [cRnE1s +H$^+$]: 3184). cRnE2s: Obsd. 3487 (Calcd. for [cRnE2s +H$^+$]: 3488). cRnE3s: Obsd. 3816 (Calcd. for [cRnE3s +H$^+$]: 3817). cRnE4s: Obsd. 4130 (Calcd. for [cRnE4s +H$^+$]: 4130).

Spectroscopic measurements

Fluorescence spectra were measured on JASCO models FP-6500 and FP-8500. The excitation wavelength was 345 nm. Band widths are 3 nm (FP-6500) or 2.5 nm (FP-8500) for excitation and emission. Before measurement, sample solutions containing DNA duplex were heated at 80°C, then slowly cooled down to 20 or 0°C at a rate of 2.5°C min^{-1}. Sample solutions contained 100 mM NaCl, 10 mM phosphate buffer, pH 7.0 and 0.2 μM donor strand (RnP1-4 or AtP1-5) and 0.4 μM acceptor strand (cRnE1-4 or cAtE1-3). For analyses of nicked and gapped duplexes, 0.2 μM donor strand (RnP1-4), 0.4 μM acceptor strand (cRnE1s-4s) and 0.6 μM Nt23-17 were used.

Measurement of melting temperatures

The melting curves were measured with a UV-1800 (Shimadzu) by monitoring 260 nm absorbance versus temperature. For nicked or gapped duplex, the melting curve was obtained with a JASCO model FP-6500 by measuring emission intensity at 500 nm with 345 nm excitation. The melting temperature (T_m) was determined from the maximum in the first derivative of the melting curve. Both the heating and the cooling curves were measured, and the calculated T_ms agreed to within 1.0°C. The temperature ramp was 0.5°C min^{-1} for absorbance or 1.0°C min^{-1} for emission. The sample solutions for melting analyses from absorbance contained 100 mM NaCl, 10 mM phosphate buffer, pH 7, 1.0 μM each DNA. The sample solutions for melting analyses from emission contained 100 mM NaCl, 10 mM phosphate buffer, pH 7, 0.2 μM donor strand (RnP1-4), 0.4 μM acceptor strand (cRnE1s-4s) and 0.6 μM Nt23-17.

Calculation of FRET efficiency

FRET efficiency (Φ_T) was experimentally determined from the decrease in donor emission:

$$\Phi_T = 1 - I_{DA}/I_D$$

where I_{DA} is emission intensity of a duplex containing a donor and an acceptor at 405 nm, and I_D is that of donor-only duplex at 405 nm. Emission intensities were measured at 20°C. Each emission intensity was normalized at the intensity of 80°C in order to eliminate the effects of concentration errors. Error bars of FRET efficiencies show standard deviations of three independent experiments.

Determination of structural parameters

FRET efficiency (Φ_T) was calculated from the following equations:

$$\Phi_T = \frac{1}{1 + (R/R_0)^6}$$

$$R_0 = 0.2108[J(\lambda)\kappa^2 n^{-4}\Phi_D]^{1/6}$$

$$\kappa^2 = (\cos\theta_T - 3\cos\theta_D\cos\theta_A)^2$$

where R is the distance between donor and acceptor, and R_0 is a Förster radius (the distance where $\Phi_T = 0.5$). $J(\lambda)$ is integral of spectral overlap between donor emission and acceptor absorption at λ nm. n is a refractive index, which is typically assumed to be 1.4 for biomolecules (26), and Φ_D is a donor quantum yield. The orientation factor, κ^2, was calculated from the above equation, where θ_T is the angle between transition dipoles of donor and acceptor, and θ_D and θ_A are the angles between these dipoles and the separation vector.

In our FRET system of duplex, donor and acceptor are in parallel planes since they are intercalated into the DNA duplex. Thus, the orientation factor is simply represented by the following equation:

$$\kappa^2 = \cos^2\theta_T$$

By using these equations, FRET efficiency can be calculated from the distance (R) and the angle (θ_T) between dyes.

For analyses of double helical structures, we used three variables, rise per base pair (a in Å), angle per base pair (b in °) and the angle between dyes and flanking base pairs (c in °). Consequently, the distance and the angle can be expressed by using the number of base pairs (n) between donor and acceptor as follows:

$$R = a \times (n+1)$$

$$\theta_T = b \times (n-1) + c$$

These three variables were determined by fitting experimental FRET efficiencies with values calculated from these equations. Values were determined from the least-squares method using Solver tool in Microsoft Excel. Errors were estimated from standard errors calculated by using KaleidaGraph (Synergy software).

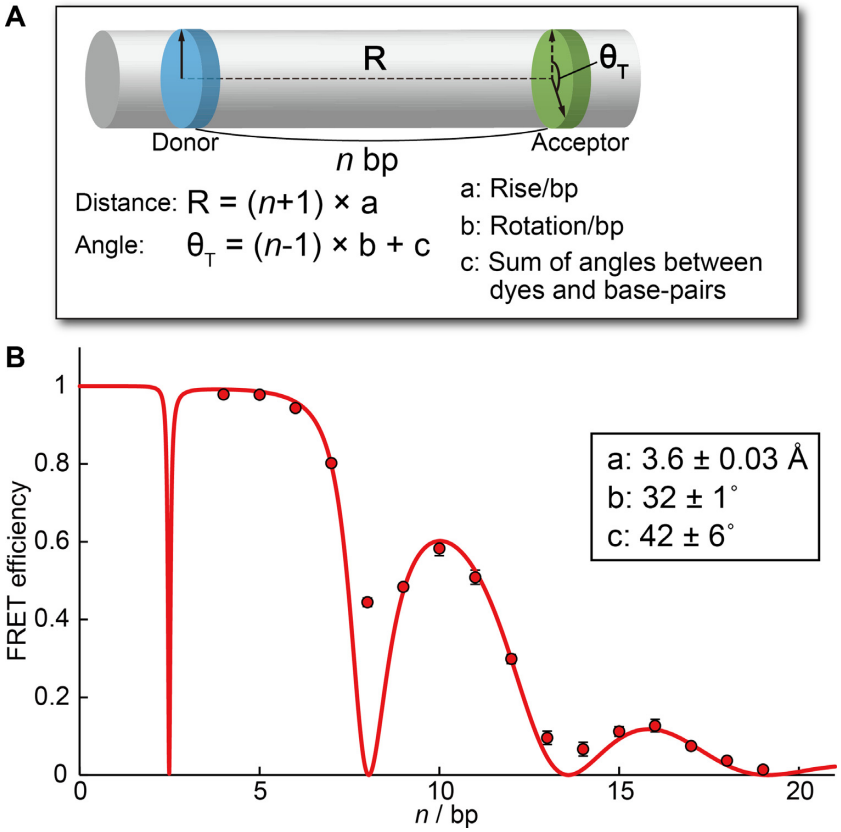

Figure 2. Analysis of structural parameters of a canonical DNA duplex. (**A**) Equations used for calculation of distance and angle between dyes. (**B**) FRET plot of a canonical DNA duplex. The x-axis is the number of base pairs between donor and acceptor. Experimental data are shown as circles. The line is FRET efficiencies theoretically calculated by using determined parameters shown in the inset.

For analyses of nicked duplex, we assumed an equilibrium between stacked and unstacked structures. In the stacked structure, the structure was assumed to be the same as that of the duplex without a nick. In unstacked duplex, a randomized orientation ($\kappa^2 = 2/3$) was assumed. Percentages of stacked and unstacked structures were estimated using the least-squares method using the Solver tool in Excel.

For analyses of duplexes with 3-nt gaps, we assumed that the orientation was not fixed and, thus, that the orientation factor (κ^2) was 2/3. The distance (R) was calculated from the following equation:

$$R = d \times (n - 2) + e$$

where d (in Å) is rise per base pair in duplexed portion of 3-nt gapped structure. And, e (in Å) is the length of 3-nt gap (i.e. the distance between duplex regions).

RESULTS AND DISCUSSION

We first analyzed the structure of a canonical duplex to validate the accuracy of our method. We synthesized four strands tethering pyrene (RnP1-4) and four complementary strands tethering perylene (cRnE1-4) shown in Figure 1. The two base pairs flanking pyrene were identical in all duplexes, and this resulted in pyrene quantum yields that were within experimental error for all duplexes (Supplementary Figure S1). The number of base pairs between the two dyes can be varied from 4 to 19 bp by combining these strands appropriately (Supplementary Table S1). We measured fluorescent emission spectra of duplexes (Supplementary Figure S2) and calculated FRET efficiencies from decrease in donor emission. FRET efficiency between dyes in canonical duplexes as a function of distance in base pairs is not monotonous, but periodic, demonstrating orientation dependence of FRET (Figure 2B). Three variables were used to calculate FRET efficiencies: rise, rotation and the sum of angles between dyes and neighboring base pairs (Figure 2A). Parameters were determined by using least-squares method. Theoretically calculated FRET efficiencies using these parameters are shown in a line in Figure 2B.

It should be noted that a large error from a theoretically calculated value was observed at 8 bp. Although we calculated FRET efficiencies by assuming that the relative angle between dyes has a Gaussian distribution, large differences at base pair separations other than 8 bp were still observed (Supplementary Figure S3). Therefore, we concluded that the difference at 8 bp was not caused by the incomplete fixation of dye orientations. It was reported based on a theoretical analysis that the point dipole approximation fails when the distance between molecules is short. Consequently, the orientation factor cannot be zero even if molecules are perpendicular (27). We believe that large difference between the experimentally determined FRET efficiency at 8 bp and the efficiency expected based on the cylindrical model is due to

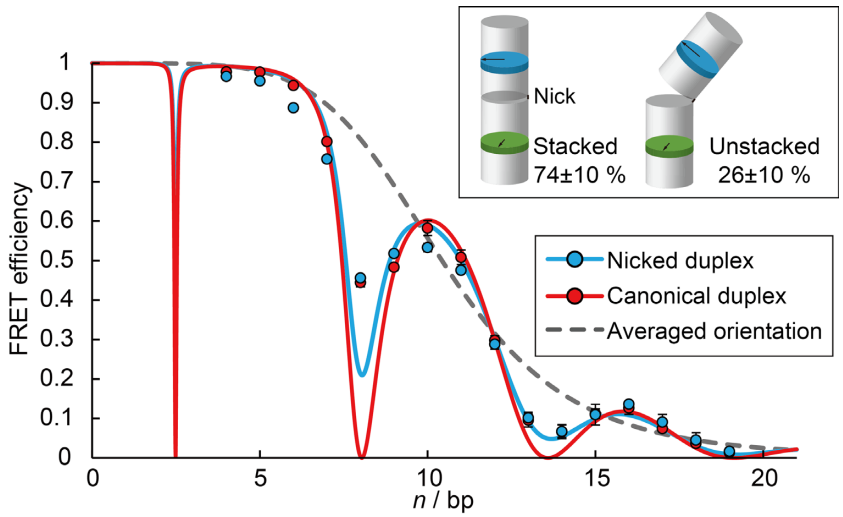

Figure 3. FRET plot of nicked (blue) and canonical (red) duplexes. The blue line curve was generated by assuming 26% of duplexes adopt an unstacked structure.

a non-zero orientation factor caused by failure of dipole approximation. From these reasons, we did not use FRET efficiency at 8 bp to determine structural parameters. For other base pair separations, experimental values agreed well with the curve generated based on the model of B-form DNA (Figure 2B), clearly demonstrating that orientation of dyes is strictly controlled in our system. The rise per base pair calculated based on FRET data was 3.6 ± 0.03 Å and rotation per base pair was 32 ± 1°, almost identical to those of a canonical B-form DNA duplex (3.4 Å and 34°, respectively). The difference of the rise could be explained by a refractive index. There is an inversely proportional relationship between the rise and the refractive index. If the refractive index is set to 1.5, rise per base pair decreases to 3.4 Å. The difference of rise per base pair indicates that the refractive index of natural base pairs are higher than 1.4. In contrast, rotation angle is not dependent on physical parameters. X-ray crystallography has shown that rotation angle is highly dependent on sequence although averaged angle is usually 34–36° (28–30). Therefore, the difference from typical rotation angle could be due to its strong sequence dependence. To the best of our knowledge, an orientation-dependent FRET system showing such an excellent agreement with theory over a long distance has not been reported previously.

We also analyzed a duplex containing an A-tract using a similar system (Supplementary Figure S4). In the case of A-tract duplex, larger differences between experimental FRET efficiencies and calculated values based on the B-form cylinder model were observed. In particular, the observed efficiencies at longer distance were higher than expected values. As reported previously, an A-tract induces a bend in DNA (31–33) so that the actual distance between donor and acceptor is shorter than expected from the cylinder model. Although more detailed investigation is required to clarify the detailed structure of A-tract, bending was clearly detected by using our FRET system.

We subsequently analyzed DNA duplexes with nicks and gaps using our FRET system. Nicked and gapped duplexes were prepared by hybridizing short acceptor-containing strands (cRnE1s-4s) and donor-containing strands (RnP1-4) with a longer DNA (Nt17-23) as shown in Figure 1. FRET efficiencies of nicked duplexes showed a non-monotonous dependence on the number of base pairs between donor and acceptor dyes (Figure 3). This indicated that the relative orientation between the donor and the acceptor was not averaged. The positions of minima and maxima in the FRET plot were the same as those of canonical duplex, showing that despite the nick, the duplex maintains a canonical B-form duplex geometry. The nicked duplex had lower maximum and higher minimum compared with canonical duplex, however. This weakened orientation dependence strongly indicated that the nick imparted flexibility. The higher flexibility of nicked duplex was also observed by using other methodologies such as gel electrophoresis and NMR (34–37). We analyzed the conformational flexibility of nicked duplex by simply assuming an equilibrium between stacked and unstacked duplex conformations (36,38). Our calculations indicated that when 26% of duplexes adopted an unstacked structure at the nick, calculated efficiencies showed better agreement with experimental values. This is a rough calculation because it is difficult to estimate the precise orientation factors of unstacked structure. However, we believe this assumption is useful to estimate relative flexibilities of various DNA structures. From these results, we concluded that a nicked duplex has higher conformational flexibility than the canonical duplex. X-ray crystallography demonstrated that nicked duplex adopts B-form duplex (39). Our study also indicates that the nicked duplex adopts a B-form conformation in solution and was able to provide a measure of the enhanced flexibility of a nicked DNA duplex relative to that of an intact duplex.

We then investigated the structure of gapped duplexes. The FRET plot of a duplex with a single nucleotide gap is shown in Figure 4A. The minima in the FRET plots were different in nicked duplexes and the duplexes with 1-nt gaps; a minimum was observed at 8 bp with the nicked duplex and at 6 nt with 1-nt gapped duplex. This shift strongly indicated

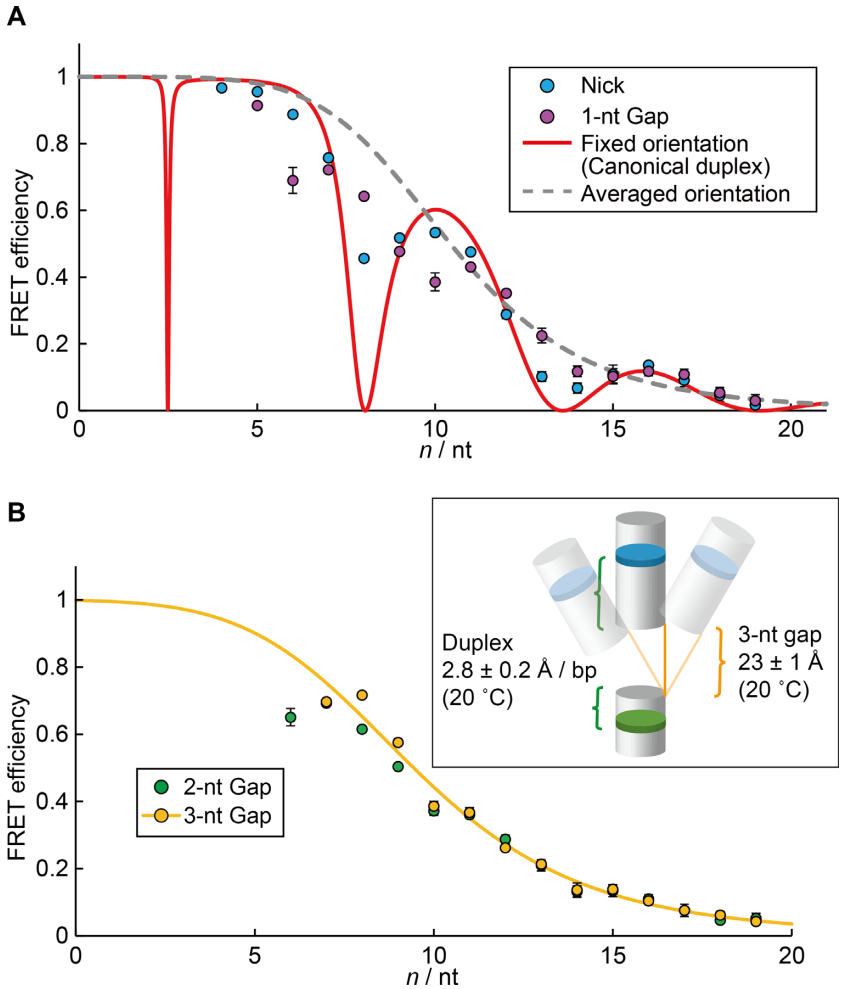

Figure 4. (**A**) FRET plots of nicked duplex and duplex with a 1-nt gap. Red line shows the fitting curve used to determine structural parameters of canonical duplex. Dotted line shows theoretical curve assuming averaged orientation of dyes in canonical duplex. (**B**) FRET plots of duplexes with 2-nt and 3-nt gaps. Curve in orange was calculated by assuming FRET efficiencies of 3-nt gapped duplexes were dependent not on orientation but on distance between dyes. Determined structural parameters of duplex with 3-nt gap at 20°C are shown in inset. See Supplementary Figure S7 for structural parameters determined from FRET efficiencies at 0°C.

that insertion of a gap altered the orientation between the two dyes. As an orientation dependence of FRET efficiency was observed with 1-nt gapped duplexes, the two duplex regions separated by a 1-nt gap are stacked. The difference in dye orientation from the nicked duplex is probably due to rotation and/or bending at the gap. Actually, NMR analysis indicated that there are two conformations with 1-nt gapped duplex; one is close to B-DNA and the other is kinked (37). Interestingly, the decline of FRET efficiency was observed at 6, 10 and 14 nt in the case of 1-nt gapped duplex. Because we used four kinds of gapped sequences as shown in Supplementary Table S4, this result indicated that structure of 1-nt gapped DNA duplex depends on its sequence.

The FRET plot of structure with the 2-nt gap showed smaller orientation dependence. FRET efficiency monotonously decreased as the number of nucleotides between the dyes increased (Figure 4B, green circles). Thus, stacking interactions between two duplexes is very weak when there is a 2-nt gap. Almost no orientation dependence was observed when the gap was 3 nt (Figure 4B, orange circles), suggesting little stacking and an averaged dye orientation. Similar results were reported by using gel electrophoresis where electrophoretic mobility decreased by insertion of two or more nucleotide gap (36,40). We estimated the length of 3-nt gap and of the complex of the three oligonucleotides by assuming a random orientation. FRET efficiencies of duplexes with 3-nt gaps were in excellent agreement with a model based on this assumption (Figure 4B, orange circles and line). The length of 3-nt gap was estimated to be 23 ± 1 Å, indicating that the gapped bases are stretched. Masuko *et al.* previously reported an equation to calculate the length of gap by using distance-dependent FRET system (6). According to their equation, the length of 3-nt gap was calculated as 19.1 Å, which is shorter than our result. We also measured emission spectra and determined FRET efficiencies at 0°C (Supplementary Figure S7). A total of 3-nt gapped duplexes at 0°C showed higher FRET efficiencies than those at 20°C, and the length of 3-nt gap at 0°C was estimated as 19 ± 2 Å. These results indicated that breathing effect of acceptor strand or high

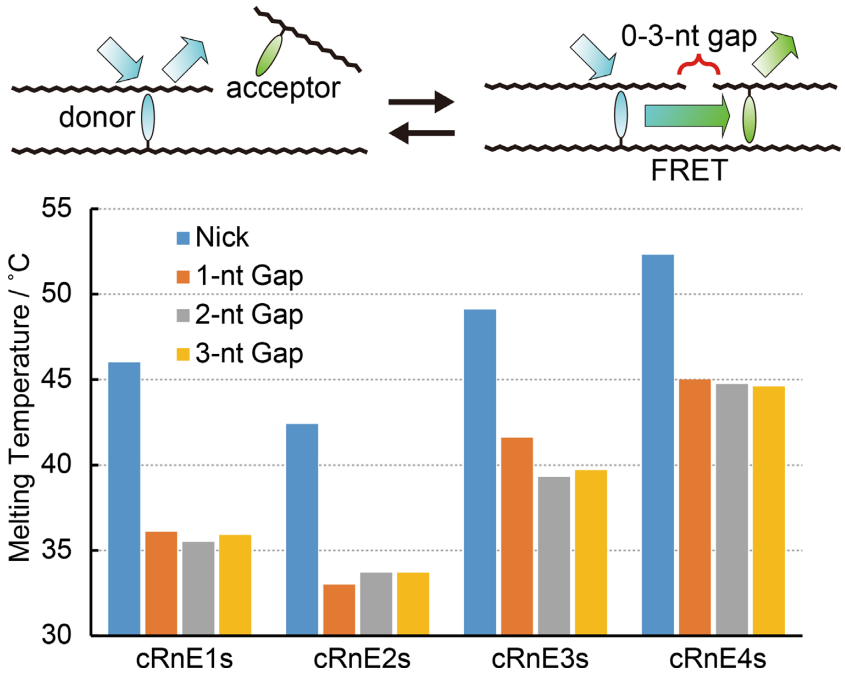

Figure 5. Melting temperatures of strand containing perylene in the context of nicked or gapped duplex. These melting temperatures were determined from melting curves obtained by monitoring 500 nm emission with 345 nm excitation such that only melting of the perylene-containing strand is observed.

mobility of 3-nt gap might contribute to the stretching of DNA. In contrast, length of double-helical portion increases by 2.8 ± 0.2 Å per base pair, which was much shorter than canonical duplex (3.6 ± 0.03 Å). The rise represents the averaged increment of the distance between a donor and an acceptor and the decrease is probably due to the movement of 3-nt gap inserted between double helixes. From these results, we concluded that two duplexes move freely when a 3-nt gap is inserted between the regions.

In order to further investigate the stacking interaction between two double helixes, melting temperatures (T_ms) of the duplexes were determined using FRET. Melting curves were obtained by monitoring emission intensity at 500 nm with excitation wavelength of 345 nm so that only hybridization of short perylene-containing strand was monitored (Supplementary Figure S8). This allowed the stacking interaction between the two helixes to be evaluated since the melting temperature of perylene-containing strand depends on whether or not the two duplexes stack. The T_ms of nicked duplexes were much higher than those of gapped duplexes, supporting our hypothesis that a stable stacking interaction occurs in the nicked duplexes (Figure 5). The T_ms of the duplexes with 1 and 2-nt gaps were within experimental error although T_m of cRnE3s slightly decreased. This result indicated that stacking interaction between two duplexes separated by 1-nt gap is weak whereas its strength partially depended on its sequence (41). Furthermore, 3-nt gapped duplexes showed same T_ms as 2-nt gaped duplexes, supporting that two duplexes are no longer stacked in those structures. Overall, the melting analyses support the conclusions drawn from FRET that the duplexes do not stack strongly when separated by a gap of 2 nt.

In conclusion, we developed a novel method for analyses of DNA structures by using the orientation-pendent FRET system. Structural parameters of canonical B-form duplex were precisely obtained by using this system. Large deviation from a cylinder model probably due to bending was observed with A-tract duplex. Moreover, differences in structures and flexibilities among nicked and gapped duplexes were revealed in detail. Although nicked duplex has high flexibility, it maintains a canonical B-form geometry. However, insertion of 1-nt gap altered the dye orientation although orientation dependence was still observed. 2-nt and 3-nt gapped duplexes showed almost no orientation dependence in FRET plot, indicating weak stacking between two duplexes separated by a gap. DNA repair enzymes, such as ligases and DNA polymerases, can recognize nicked or gapped duplexes, although the recognition of gaps depends on the gap size (42–45). Differences in structure and flexibility, which were revealed in this study, likely enable recognition by these enzymes. Importantly, our results demonstrated that the orientation of dyes is strictly controlled in our FRET system. Furthermore, other dye pairs can be incorporated into DNA via D-threoninol. We believe our FRET system will prove to be a facile and versatile tool for analysis of DNA structures in solution. This system could, for example, be used to analyze structures of DNA duplexes with various types of damage, such as radiation-induced lesions, epigenetically modified nucleobases and non-natural molecules (46,47). Moreover, structural changes in DNA duplexes induced by protein binding could be analyzed using this FRET system.

SUPPLEMENTARY DATA

Supplementary Data are available at NAR Online.

FUNDING

PRESTO from Japan Science and Technology Agency; JSPS KAKENHI [JP16H05925, JP25248037]; The Asahi Glass Foundation. Funding for open access charge: The Asahi Glass Foundation.
Conflict of interest statement. None declared.

REFERENCES

1. Yang,W. (2008) Structure and mechanism for DNA lesion recognition. *Cell Res.*, **18**, 184–197.
2. Germann,M.W., Johnson,C.N. and Spring,A.M. (2012) Recognition of damaged DNA: structure and dynamic markers. *Med. Res. Rev.*, **32**, 659–683.
3. Clegg,R.M. (1992) [18]Fluorescence resonance energy transfer and nucleic acids. *Methods Enzymol.*, **211**, 353–388.
4. Preus,S. and Wilhelmsson,L.M. (2012) Advances in quantitative FRET-based methods for studying nucleic acids. *Chembiochem*, **13**, 1990–2001.
5. Norman,D.G., Grainger,R.J., Uhrin,D. and Lilley,D.M.J. (2000) Location of cyanine-3 on double-stranded DNA: importance for fluorescence resonance energy transfer studies. *Biochemistry*, **39**, 6317–6324.
6. Masuko,M., Ohuchi,S., Sode,K., Ohtani,H. and Shimadzu,A. (2000) Fluorescence resonance energy transfer from pyrene to perylene labels for nucleic acid hybridization assays under homogeneous solution conditions. *Nucleic Acids Res.*, **28**, e34.
7. Widengren,J., Schweinberger,E., Berger,S. and Seidel,C.A.M. (2001) Two new concepts to measure fluorescence resonance energy transfer via fluorescence correlation spectroscopy: theory and experimental realizations. *J. Phys. Chem. A*, **105**, 6851–6866.
8. Dietrich,A., Buschmann,V., Müller,C. and Sauer,M. (2002) Fluorescence resonance energy transfer (FRET) and competing processes in donor–acceptor substituted DNA strands: a comparative study of ensemble and single-molecule data. *Rev. Mol. Biotechnol.*, **82**, 211–231.
9. Lee,S., Lee,J. and Hohng,S. (2010) Single-molecule three-color FRET with both negligible spectral overlap and long observation time. *PLoS One*, **5**, e12270.
10. Di Fiori,N. and Meller,A. (2010) The effect of dye-dye interactions on the spatial resolution of single-molecule FRET measurements in nucleic acids. *Biophys. J.*, **98**, 2265–2272.
11. Kupstat,A., Ritschel,T. and Kumke,M.U. (2011) Oxazine dye-conjugated DNA oligonucleotides: förster resonance energy transfer in view of molecular dye–DNA interactions. *Bioconjug. Chem.*, **22**, 2546–2557.
12. Forster,T. (1946) Energiewanderung und fluoreszenz. *Naturwissenschaften*, **33**, 166–175.
13. Woźniak,A.K., Schröder,G.F., Grubmüller,H., Seidel,C.A.M. and Oesterhelt,F. (2008) Single-molecule FRET measures bends and kinks in DNA. *Proc. Natl. Acad. Sci. U.S.A.*, **105**, 18337–18342.
14. Lewis,F.D., Zhang,L. and Zuo,X. (2005) Orientation control of fluorescence resonance energy transfer using DNA as a helical scaffold. *J. Am. Chem. Soc.*, **127**, 10002–10003.
15. Iqbal,A., Arslan,S., Okumus,B., Wilson,T.J., Giraud,G., Norman,D.G., Ha,T. and Lilley,D.M.J. (2008) Orientation dependence in fluorescent energy transfer between Cy3 and Cy5 terminally attached to double-stranded nucleic acids. *Proc. Natl. Acad. Sci. U.S.A.*, **105**, 11176–11181.
16. Börjesson,K., Preus,S., El-Sagheer,A.H., Brown,T., Albinsson,B. and Wilhelmsson,L.M. (2009) Nucleic acid base analog FRET-pair facilitating detailed structural measurements in nucleic acid containing systems. *J. Am. Chem. Soc.*, **131**, 4288–4293.
17. Preus,S., Kilså,K., Miannay,F.-A., Albinsson,B. and Wilhelmsson,L.M. (2013) FRETmatrix: a general methodology for the simulation and analysis of FRET in nucleic acids. *Nucleic Acids Res.*, **41**, e18.
18. Fessl,T. and Lilley,D.M.J. (2013) Measurement of the Change in twist at a helical junction in RNA using the orientation dependence of FRET. *Biophys. J.*, **105**, 2175–2181.
19. Kato,T., Kashida,H., Kishida,H., Yada,H., Okamoto,H. and Asanuma,H. (2013) Development of a robust model system of FRET using base surrogates tethering fluorophores for strict control of their position and orientation within DNA duplex. *J. Am. Chem. Soc.*, **135**, 741–750.
20. Kashida,H., Liang,X.G. and Asanuma,H. (2009) Rational design of functional DNA with a non-ribose acyclic scaffold. *Curr. Org. Chem.*, **13**, 1065–1084.
21. Sancar,A., Lindsey-Boltz,L.A., Ünsal-Kaçmaz,K. and Linn,S. (2004) Molecular mechanisms of mammalian DNA repair and the DNA damage checkpoints. *Annu. Rev. Biochem.*, **73**, 39–85.
22. Lindahl,T. and Wood,R.D. (1999) Quality control by DNA repair. *Science*, **286**, 1897–1905.
23. Liang,X., Asanuma,H., Kashida,H., Takasu,A., Sakamoto,T., Kawai,G. and Komiyama,M. (2003) NMR Study on the photoresponsive DNA tethering an azobenzene. Assignment of the absolute configuration of two diastereomers and structure determination of their duplexes in the trans-form. *J. Am. Chem. Soc.*, **125**, 16408–16415.
24. Asanuma,H., Akahane,M., Kondo,N., Osawa,T., Kato,T. and Kashida,H. (2012) Quencher-free linear probe with multiple fluorophores on an acyclic scaffold. *Chem. Sci.*, **3**, 3165–3169.
25. Doi,T., Sakakibara,T., Kashida,H., Araki,Y., Wada,T. and Asanuma,H. (2015) Hetero-selective DNA-like duplex stabilized by donor–acceptor interactions. *Chem. Eur. J.*, **21**, 15974–15980.
26. Lakowicz,J.R. (2006) *Principles of Fluorescence Spectroscopy*. Springer, NY.
27. Muñoz-Losa,A., Curutchet,C., Krueger,B.P., Hartsell,L.R. and Mennucci,B. (2009) Fretting about FRET: failure of the ideal dipole approximation. *Biophys. J.*, **96**, 4779–4788.
28. Dickerson,R.E. and Drew,H.R. (1981) Structure of a B-DNA dodecamer. *J. Mol. Biol.*, **149**, 761–786.
29. Larsen,T.A., Kopka,M.L. and Dickerson,R.E. (1991) Crystal structure analysis of the B-DNA dodecamer CGTGAATTCACG. *Biochemistry*, **30**, 4443–4449.
30. Grzeskowiak,K. (1996) Sequence-dependent structural variation in B-DNA. *Chem. Biol.*, **3**, 785–790.
31. Wu,H.-M. and Crothers,D.M. (1984) The locus of sequence-directed and protein-induced DNA bending. *Nature*, **308**, 509–513.
32. Nelson,H.C.M., Finch,J.T., Luisi,B.F. and Klug,A. (1987) The structure of an oligo(dA)·oligo(dT) tract and its biological implications. *Nature*, **330**, 221–226.
33. DiGabriele,A.D. and Steitz,T.A. (1993) A DNA Dodecamer containing an adenine tract crystallizes in a unique lattice and exhibits a new bend. *J. Mol. Biol.*, **231**, 1024–1039.
34. Furrer,P., Bednar,J., Stasiak,A.Z., Katritch,V., Michoud,D., Stasiak,A. and Dubochet,J. (1997) Opposite effect of counterions on the persistence length of nicked and non-nicked DNA1. *J. Mol. Biol.*, **266**, 711–721.
35. Zhang,Y. and Crothers,D.M. (2003) High-throughput approach for detection of DNA bending and flexibility based on cyclization. *Proc. Natl. Acad. Sci. U.S.A.*, **100**, 3161–3166.
36. Yakovchuk,P., Protozanova,E. and Frank-Kamenetskii,M.D. (2006) Base-stacking and base-pairing contributions into thermal stability of the DNA double helix. *Nucleic Acids Res.*, **34**, 564–574.
37. Roll,C., Ketterlé,C., Faibis,V., Fazakerley,G.V. and Boulard,Y. (1998) Conformations of nicked and gapped DNA structures by NMR and molecular dynamic simulations in water. *Biochemistry*, **37**, 4059–4070.
38. Protozanova,E., Yakovchuk,P. and Frank-Kamenetskii,M.D. (2004) Stacked–unstacked equilibrium at the nick site of DNA. *J. Mol. Biol.*, **342**, 775–785.
39. Aymami,J., Coll,M., van der Marel,G.A., van Boom,J.H., Wang,A.H. and Rich,A. (1990) Molecular structure of nicked DNA: a substrate for DNA repair enzymes. *Proc. Natl. Acad. Sci. U.S.A.*, **87**, 2526–2530.
40. Mills,J.B., Cooper,J.P. and Hagerman,P.J. (1994) Electrophoretic evidence that single-stranded regions of 1 or more nucleotides dramatically increase the flexibility of DNA. *Biochemistry*, **33**, 1797–1803.
41. The 1-nt gapped duplex of cRnE3s has consecutive two thymidines at the gapped site (see Table S4 for actual sequence). This duplex can adopt a bulge like structure rather than a gapped structure. We believe this structure contribute to the relatively high stability of 1-nt gapped duplex with cRnE3s.

42. Brown,J.A., Pack,L.R., Sanman,L.E. and Suo,Z. (2011) Efficiency and fidelity of human DNA polymerases λ and β during gap-filling DNA synthesis. *DNA Repair*, **10**, 24–33.
43. Karimi-Busheri,F., Lee,J., Weinfeld,M. and Tomkinson,A.E. (1998) Repair of DNA strand gaps and nicks containing 3′-phosphate and 5′-hydroxyl termini by purified mammalian enzymes. *Nucleic Acids Res.*, **26**, 4395–4400.
44. Ho,C.K., Van Etten,J.L. and Shuman,S. (1997) Characterization of an ATP-dependent DNA ligase encoded by Chlorella virus PBCV-1. *J. Virol.*, **71**, 1931–1937.
45. Liu,Y., Beard,W.A., Shock,D.D., Prasad,R., Hou,E.W. and Wilson,S.H. (2005) DNA polymerase β and flap endonuclease 1 enzymatic specificities sustain DNA synthesis for long patch base excision repair. *J. Biol. Chem.*, **280**, 3665–3674.
46. Gates,K.S. (2009) An overview of chemical processes that damage cellular DNA: spontaneous hydrolysis, alkylation, and reactions with radicals. *Chem. Res. Toxicol.*, **22**, 1747–1760.
47. Carell,T., Brandmayr,C., Hienzsch,A., Müller,M., Pearson,D., Reiter,V., Thoma,I., Thumbs,P. and Wagner,M. (2012) Structure and function of noncanonical nucleobases. *Angew. Chem. Int. Ed.*, **51**, 7110–7131.